Effects of hot forging on the structural condition in HS 6-5-2 high-speed steel

IOP Conf. Series: Materials Science and Engineering **723** (2020) 012002 doi:10.1088/1757-899X/723/1/012002

Effects of hot forging on the structural condition in HS 6-5-2 high-speed steel

V Průcha[1], S Benešová[1], V Veselý[1], M Kesl[2]

[1]Department of Material Science and Technology University of West Bohemia. Univerzitní 8, 301 00 Plzeň, Czech Republic.

[2]Pilsen Tools s.r.o., Tylova 1/57, 301 00 Plzeň, Czech Republic.

E-mail: vprucha@kmm.zcu.cz

Abstract. Microstructure analysis was performed on rolled bars of high-speed steel after two and three forging cycles, each cycle comprising one upsetting and one drawing out operation. High-speed steels belong to difficult-to-form materials with a narrow forging temperature interval. Forging above the maximum forging temperature may lead to grain coarsening. Below the minimum forging temperature, deformation resistance of the material increases, and the workpiece may fail. Using numerical modelling, special forging dies were designed and effective strain distribution was calculated for an axial cross-section plane in specimens after two and three forging cycles. The purpose of the analysis was to identify the relationship between the amount of effective strain and the shape and size of austenite grain and the volume fraction and density of carbides after forging. The size of prior austenite grains was measured using the linear intercept method which is based on the Snyder-Graff method. Grain shapes were characterized in terms of circularity, which is the difference between the shape in question and a circle. With increasing amount of strain, the grains in the material became finer, as undissolved carbides impeded grain growth. In as-received rolled condition, the austenite grain size was G9. After three forging cycles, it was smaller, G11 (the higher the number, the smaller the grains). Circularity characterizes the complexity of a grain shape. Micrographs of carbide particles were taken using a scanning electron microscope and examined with NIS Elements image analysis software. The majority of carbides were sized between 0.2 and 2 μm. The carbides which are less than 1 μm in size do not shrink in response to increasing strain and their quantity does not change appreciably. Carbides with a size of 1-2 μm show a different behaviour. In the central region of specimens, where strain is the largest, their amounts are much larger than in less-worked regions.

1. Introduction

Although steel is traditionally worked by forging, lack of information persists in terms of the relationship between the microstructural conditions of high-speed steels (HSS) and the amount of strain in a forged workpiece. High-speed steels are characterized by the presence of various carbides [1]. In addition to chromium carbides, they contain complex carbides of molybdenum, tungsten and vanadium. Some carbides dissolve during hot forming (e.g. Fe_3C and $Cr_{23}C_6$), whereas others are stable (M_6C, M_7C_3, M_2C, MC and M_4C_3) and become crushed, fragmented and shifted around. Undissolved carbides prevent grain growth during hot forming and contribute to microstructure refinement [2].

High-speed steels are air-hardenable but they may suffer quench cracks when cooled rapidly from finish forging temperatures. Carbides provide good cutting performance and abrasion resistance. Toughness and resistance to tempering are given by the condition of the matrix after forming and subsequent quenching and tempering [3]. This paper explores the relationship between the amount of deformation introduced into high-speed molybdenum steel HS 6-5-2, DIN 1.3343 (equivalent ČSN 419830 grade) by alternate hot upsetting and elongation out and the prior austenite grain size and shapes. Chemical composition of the steel is shown in table 1.

Table 1. Chemical composition of HS 6-5-2 steel.

Wt. [%]	C	Mn	Si	P	S	Cr	Mo	W	V
	0.80-0.90	max. 0.45	max. 0.45	max. 0.035	max. 0.035	3.80-4.60	4.50-5.50	5.50-7.00	1.50-2.20

Alternate upsetting and elongation out is a sequence of forging operations which successively cause the material to flow in all three orthogonal directions in each cycle, the directions of the flow being opposite in consecutive cycles. As a result, these repetitive cycles ultimately bring the individual locations within the workpiece more or less back to their initial locations. High-speed steels are difficult-to-form materials with a narrow range of forging temperatures from 1150°C to 900°C [4, 5]. In this range, their flow stress may reach 350 MPa, the same as the ultimate strength of ordinary steels at room temperature.

2. Experiments

The specimens were 1.3 kg slugs from rolled bars 50 mm in diameter and 75 mm in height in soft annealed condition. Forging was performed in CKW 6000 programmable laboratory forging press of 1 MN capacity, which offers programmable forging speeds. The specimens were heated in a two-chamber electrical resistance furnace. One chamber was kept at 700°C. The other chamber maintained the upper forging temperature, 1150°C. The chamber at 700°C was used for pre-heating and reheating. This material is relatively difficult to form and the temperature of specimens decreases during forging. This places demands on the speed of processing and handling operations. During the forging process, the forging time of a batch of eight specimens was monitored to ensure that it does not exceed 15 minutes. Hence, the time available for forging a single piece was no more than two minutes. Since forging was performed manually, it is not possible to determine the exact process time. Between individual operations, the specimens were placed in the furnace at 700°C. Before each forging operation, the specimens were transferred to the furnace at 1150°C. After the specimens had been placed in the furnace, the temperature inside the chamber decreased. Once the furnace had returned to the upper forging temperature, the specimens were held for five minutes to ensure that they heat through before forging. After all forging operations, the specimens were left to cool in the furnace to approx. 60°C for several dozen hours to prevent quenching and to obtain material which is easy to cut and machine.

Metallographic sections through the specimens were prepared and photographed using Zeiss Vert.A1 optical microscope. The prior austenite grain boundaries were difficult to reveal due to the complexity of the matrix in this high-speed steel. The matrix of perlite and ferrite was effectively etched with Nital (100 ml C_2H_5OH + 3 ml HNO_3). The complex matrix of martensite, bainite and pearlite resulting from transformations after cooling in furnace was etched with a reagent specified in ČSN EN ISO 643 (42 0462) standard. This etchant consisted of a saturated aqueous solution of picric acid and sodium alkyl sulfonate mixed at 5:1 ratio and heated to 60°C. Neither of the above etching reagents revealed prior austenite grains in the rolled and annealed sample (as-received condition). This obstacle was removed by oil quenching the sample from 1220°C and subsequent etching with Nital. Magnifications for grain size measurement are prescribed by ISO 643:2012 standard. At least 50 particles must be measured. In each case, measurements were taken on five micrographs. The same measurement was performed for determining the shape factor of grains. For

analysis of carbides was also used PHILIPS 30XL ESEM scanning electron microscope, the BSE mode, magnification 2000×. Carbides were revealed by etching with Vilella-Bain reagent (100 ml C_2H_5OH + 5 ml HCl + 1 g $C_6H_3N_3O_7$). The amount of carbides in the matrix was evaluated using image analysis software NIS – Elements AR v. 4.40. Carbide particle were also counted within intervals of their equivalent diameter. These intervals were 0.1 µm for particles smaller than 1 µm, and 1 µm for those larger than 1 µm. The ISO 16 232-7 standard deals with particle sizes which can be analysed. Depending on current image calibration, it defines objects five-fold larger than the image calibration factor as acceptable for analysis [6]. With images captured at 2000× magnification, the image calibration factor was 0.04 µm/pixel. Therefore the smallest particles to be considered were 200 nm in size [7] which is sufficient in the present case. 15 micrographs from each location were used for the measurement. The aggregate area measured was 34800 µm^2.

3. Results and discussion

3.1 Numerical modelling and boundary conditions

Effective strain fields in specimens subjected to two and three forging cycles were computed using FE simulation DEFORM software [8] according to equation:

$$\varepsilon_{ef} = \sqrt{2/3}\left[(\varepsilon_1-\varepsilon_2)^2+(\varepsilon_2-\varepsilon_3)^2+(\varepsilon_3-\varepsilon_1)^2\right]^{1/2} \quad (1)$$

Where ε_1, ε_2 and ε_3 denote principal strains. The amount of effective strain in the input stock was considered zero. The calculation therefore only covered the strain introduced by the forging cycle. Materials data, i.e. flow stress curves, thermal conductivity, specific heat capacity and the friction and heat transfer equations were adopted from the literature [9, 10]. Based on these simulations, three pairs of forging dies were designed which were intended to prevent spreading of the forged specimen. When the specimen spreading is restricted by the die walls, tensile stresses are reduced. These stresses normally occur when the specimen buckles, and lead to cracking along the circumference of the disc being upset [11]. Effective strain distribution on a central cross-section plane according to numerical modelling of two and three cycles is shown in figure 1. The locations in which microstructure was examined and which received the largest and smallest deformation were denoted as P1 and P2, respectively. Location P2 is in a peripheral region of the specimen, with low strains when compared to the specimen centre, despite repeated forging operations. Effective strains in P1 were ε_{ef} = 8.1 for two forging cycles and ε_{ef} = 9.9 for three cycles. In location P2, the values were ε_{ef} = 1.6 for two forging cycles and ε_{ef} = 3.2 for three forging cycles, as illustrated in figure 1.

a)

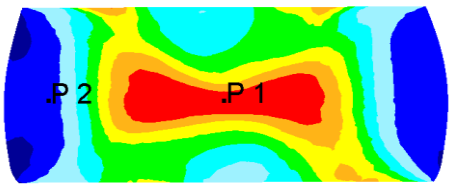

2 cycles		
location	P1	P2
ε_{ef}	8.1	1.6

b)

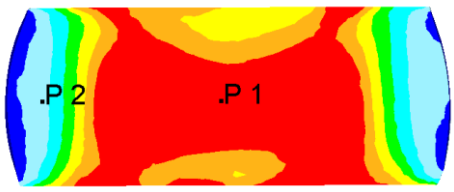

3 cycles		
location	P1	P2
ε_{ef}	9.9	3.2

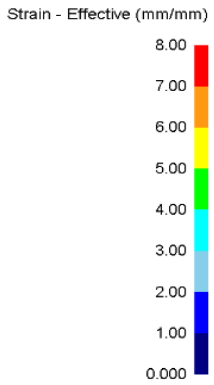

Figure 1. Effective strain distribution on a longitudinal cross section through the specimen centre, as found by numerical simulations of a) two forging cycles and b) three forging cycles.

3.2 Evaluation of prior austenite grains

The prior austenite grain size in HS 6-5-2 DIN 1.3343 steel (ČSN EN 41 9830) was determined using the linear intercept method according to ČSN EN ISO 643 "Steels - Micrographic determination of the apparent grain size", which is based on the Snyder-Graff method [12]. The measurement involves superposing line segments in three directions onto a micrograph. Grain size is indicated with letter G and a number. Higher numbers after the letter G indicate that the grains are finer. For the sake of comparison, measurements were also taken on as-received rolled and annealed specimens. The results are listed in table 2. The microstructure grew finer with increasing amount of deformation. However, refinement only became noticeable when the material undergoes effective strain higher than approximately 3 ($\varepsilon_{ef} \geq 3$). In the centre of the heavily-forged specimen ($\varepsilon_{ef} \approx 10$), the grain size was G11.

Table 2. Prior austenite grain size.

Specimen	Initial condition	Two forging cycles, point P2 (peripheral region)	Three forging cycles, point P2 (peripheral region)	Three forging cycles, point P1 (centre)
Effective strain ε_{ef}	-	1.6	3.2	9.9
Grain size - ČSN EN 41 9830	G9	G9	G9-10	G11
Grain size [μm]	12.8 ± 1.1	13.7 ± 1.2	12.2 ± 0.5	6.5 ± 0.4

3.3 Evaluation of circularity of austenite grains

The other grain characteristic assessed in this work was the shape factor. It is a dimensionless quantity which indicates the difference between the shape of an element and an ideal user-defined shape. In this case, the ideal shape was a circle. The calculation followed the equation:

$$f = \frac{4\pi A}{L^2} \qquad (2)$$

Where L denotes the circumference of the particle under measurement and A is the area of the particle. The interval of shape factor values is 0-1. The lower the shape factor is (circularity in this case), the greater is the virtual distance of the particle's shape from the ideal shape [13].

Results of measurement are plotted and relevant micrographs in as-received and forged conditions are shown in figures 2 - 5. In as-received material, most grains exhibit circularity in the range of 0.65–0.75. Strong carbide banding [3] was present and had impact on the final shapes of grains after annealing and quenching. The purpose of these heat treating operations was to reveal austenite grains (figure 2). In the peripheral region of the specimen which was worked with two forging cycles, where $\varepsilon_{ef} = 1.6$, most grains exhibited circularities of 0.7–0.75. Along with them, there were more grains with circularities between 0.5 and 0.55; and the histogram broadened because significantly non-circular grains had emerged. This trend grew stronger with increasing amounts of deformation. As a result, in the peripheral region of the specimen after three forging cycles (where $\varepsilon_{ef} = 3.2$), the largest percentage of grains showed a circularity of 0.55 to 0.7. The variance of grain circularity values also became larger. The central region with strain level $\varepsilon_{ef} = 9.9$ in the specimen which had been worked with three forging cycles contained a large number of considerably non-circular grains. Each of the five circularity classes between 0.4 and 0.7 comprised almost equal number of grains. At high strains,

very non-circular grains formed in the microstructure. These were rarely found in the as-received material.

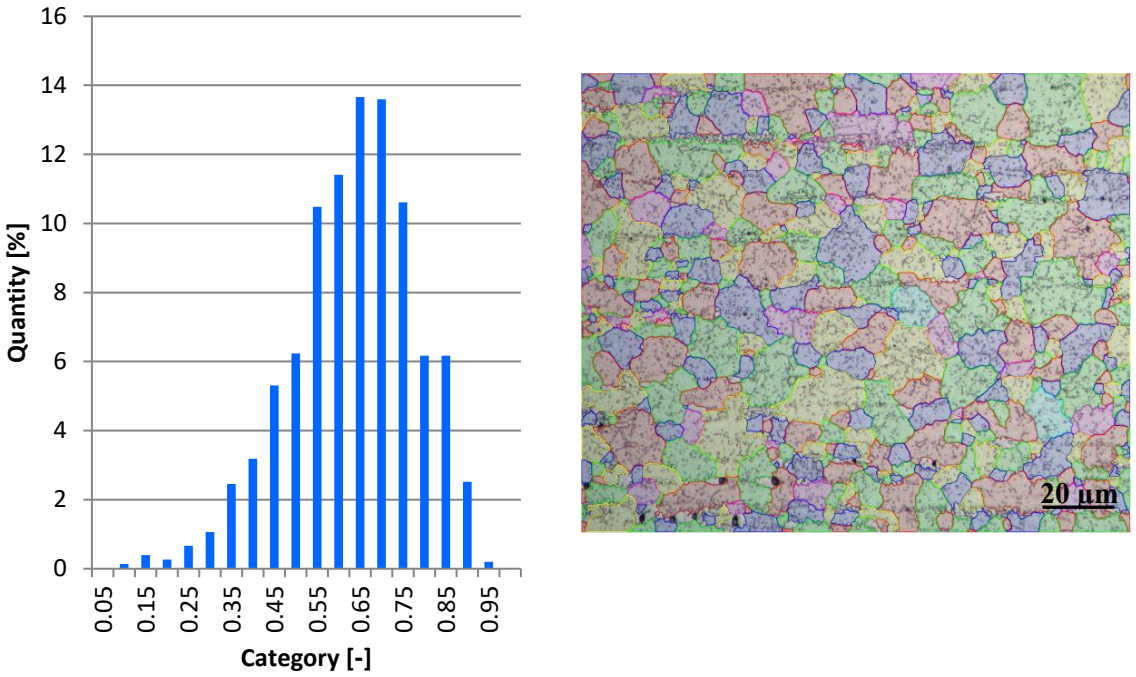

Figure 2. Circularity of prior austenite grains- as-received rolled condition, longitudinal cross-section.

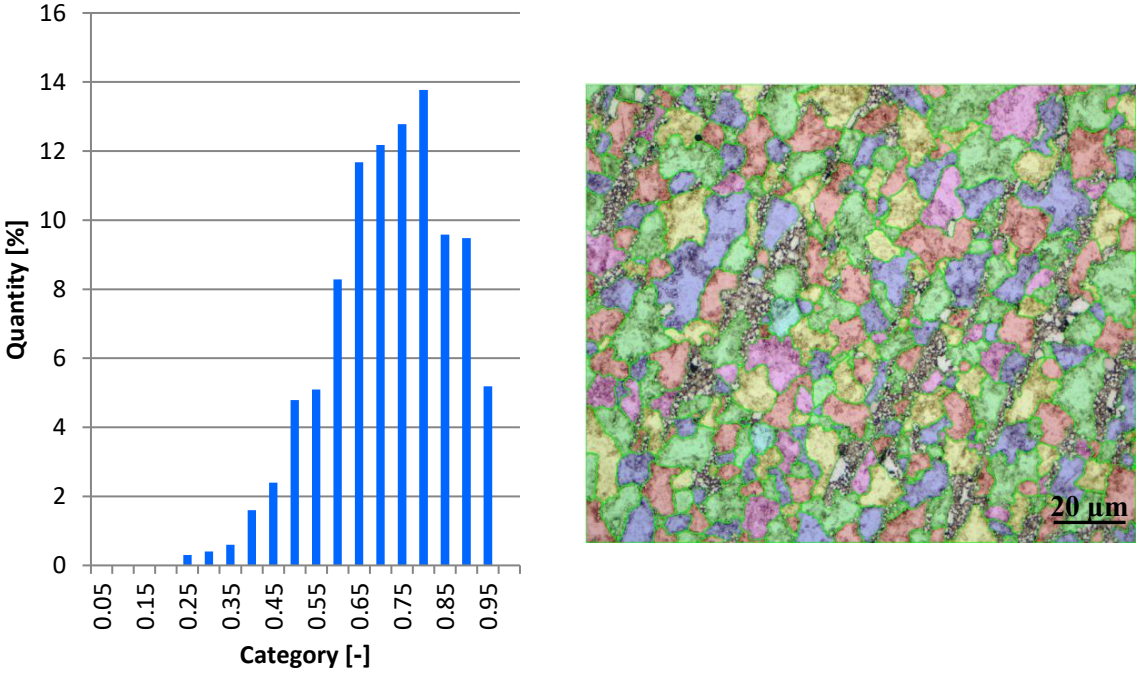

Figure 3. After 2 forging cycles, location P3 (periphery), ε_{ef}= 1.6.

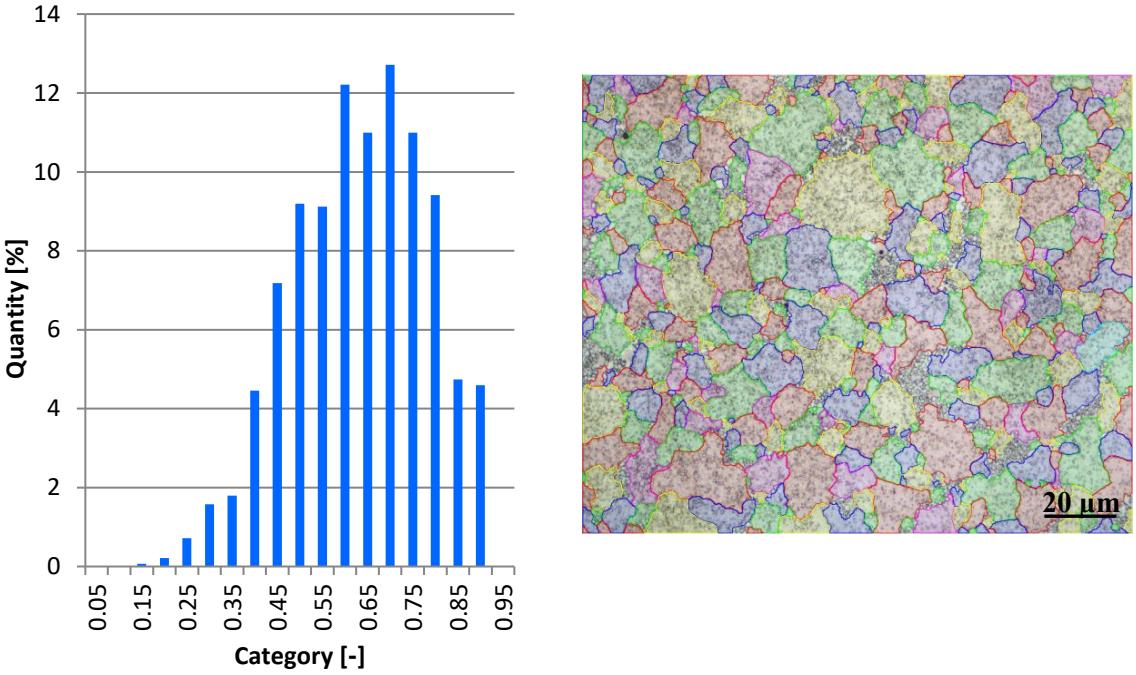

Figure 4. Circularity of prior austenite grains - 3 forging cycles, location P2 (periphery), $\varepsilon_{ef} = 3.2$.

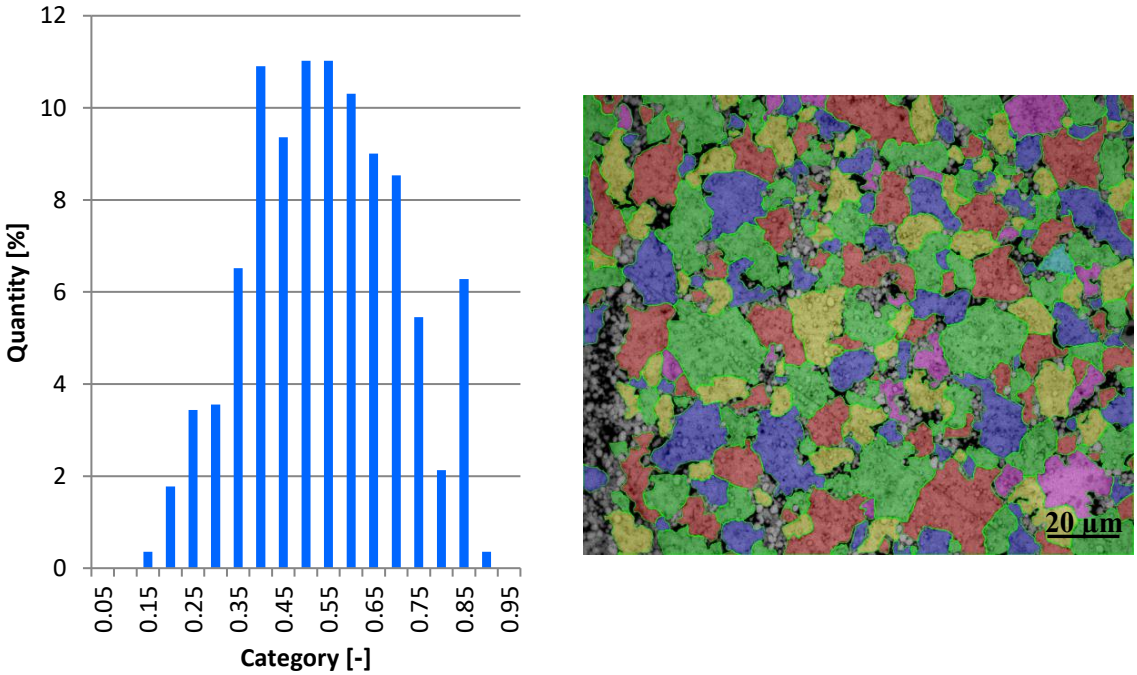

Figure 5. After three forging cycles, point P1 (centre), $\varepsilon_{ef} = 9.9$.

3.4 The size and frequency of carbides

Figure 6 shows the distribution of carbides in the location with the smallest deformation, $\varepsilon_{ef} = 1.6$ (left) and the location of the largest deformation $\varepsilon_{ef} = 9.9$ (right). They clearly show that in the specimen which was subjected to two forging cycles, the peripheral region ($\varepsilon_{ef} = 1.6$) contain large clusters of carbides, which are not present in the central region with high deformation of the specimen forged in three cycles ($\varepsilon_{ef} = 9.9$).

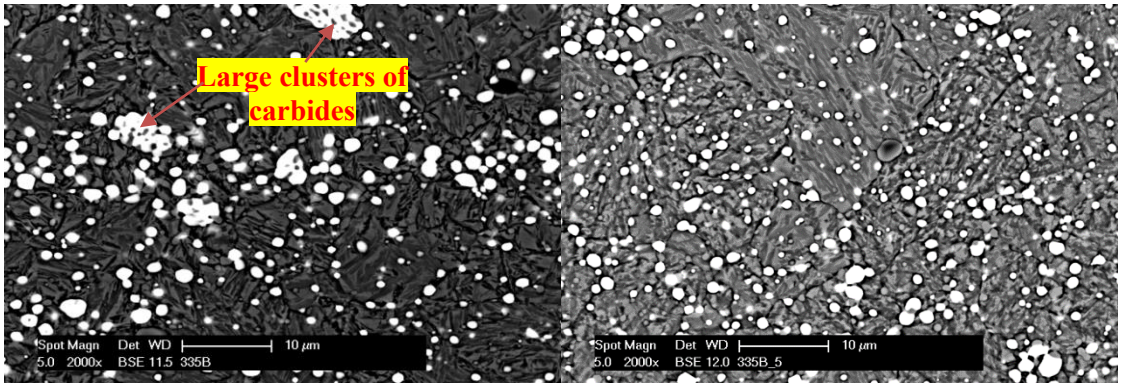

Figure 6. Distribution of carbides in martensitic matrix (in selected specimens): left – two forging cycles, region P2 (peripheral region of the specimen - $\varepsilon_{ef} = 1.6$); right - three forging cycles, region P1 (specimen centre - $\varepsilon_{ef} = 9.9$).

Figure 7 shows a histogram of equivalent diameters of carbides in specimens forged in two cycles. The location on the left is P2 (periphery of the specimen - $\varepsilon_{ef} = 1.6$), in which the fraction of the carbide phase was found to be 15.2 ± 4.5%. The location on the right is P1 (centre of the specimen - $\varepsilon_{ef} = 8.1$), in which the fraction of the carbide phase was found to be 18.9 ± 3.4%.

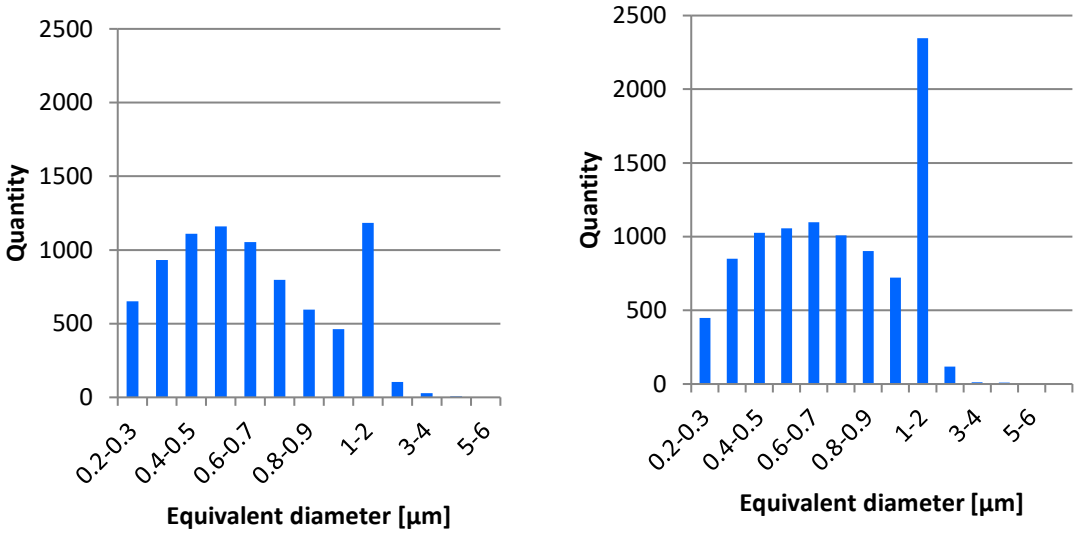

Figure 7. Histograms of equivalent diameters of carbide particles for samples with 2 forging cycles. Left: region P2 (periphery - $\varepsilon_{ef} = 1.6$); right: region P1 (centre - $\varepsilon_{ef} = 8.1$).

Figure 8 shows a histogram of the equivalent diameters of carbides in specimens forged in three cycles. The location on the left is P2 (periphery of the specimen - $\varepsilon_{ef} = 3.2$), in which the fraction of

the carbide phase was found to be 14.6 ± 4.7 %. The location on the right is P1 (centre of the specimen - ε_{ef} = 9.9), in which the fraction of the carbide phase was found to be 17.7 ± 4.1 %.

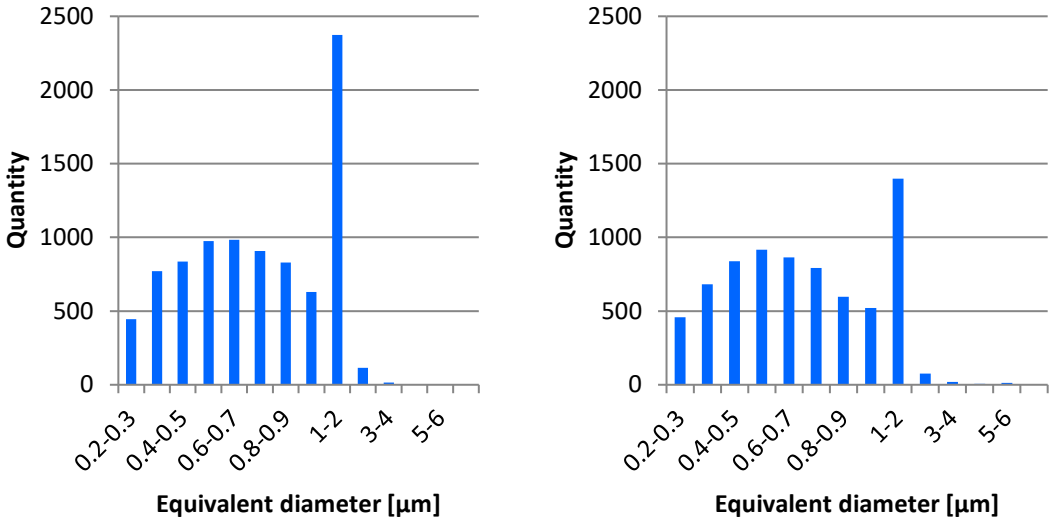

Figure 8. Histograms for samples with 3 forging cycles. Left: region P2 (periphery - ε_{ef} = 3.2); right: region P1 (centre - ε_{ef} = 9.9).

Carbides between 2 and 5 µm are only found in small amounts. In both cases, they are not likely to have a substantial effect on material properties, owing to their low counts.

The amounts of carbides 1-2 µm in size vary. In the highly deformed centres of specimens forged in two and three cycles, their counts are nearly identical. After conversion, they are approx. 660/10000 µm^2. In the peripheral region of the specimen after three cycles, their density was a mere 400/10000 µm^2. In the peripheral region of the specimen processed with two cycles, it was no more than 345/10000 µm^2.

The fractions and distributions of carbides smaller than 1 µm, i.e. sized 0.2 to 1 µm, are very similar in all the specimens forged. Their maximum is in the 0.4–0.8 µm range, where their counts are at 900–1100 in the area under examination.

4. Conclusion

The goal of this experimental work was to assess the impact of forging on prior austenite grains and on the volume fraction, sizes and distribution of carbides in relation to the effective strain field in high-speed steel HS 6-5-2 (according to ČSN 41 9830). The first location is the centre with the largest strain ε_{ef} = 8.1 (after two forging cycles) and ε_{ef} = 9.9 (after three forging cycles). Another location, the least worked one, was at the periphery of the specimen, with a strain of ε_{ef} = 1.6 after two forging cycles and ε_{ef} = 3.2 after three cycles.

The grains were found to shrink with increasing strain: from G9 in the as-received rolled condition to G11 in the heavily-forged specimen. The size of austenite grains influenced the size of grains of other phases. Post-forging heat treatment produced complex, very fine and highly-stable microstructures. Grain refinement led to higher grain boundary densities. The boundaries became obstacles to dislocation movement, which was reflected in material strengthening, specifically higher yield strength (Re). With increasing deformation, the numbers of strongly non-circular grains were rising. In addition, the amount of lattice defects, including the spatial ones, one of which are grain boundaries, increased with the amount of strain. Circularity of austenite grains was decreasing, which means that the total area of grain boundaries expanded.

It was found that larger carbides break up and become finer during upsetting of the rolled material. However after breaking and refining as the forging process continues and strain accumulates, their size remains unchanged, and only their positions change. They prevent austenite grain growth and affect the complexity of the grain shape.

In addition, the area fraction of carbides in peripheral regions was lower than in the centre, due to the smaller proportion of carbides sized 1–2 μm. Forging temperatures under 1150 °C are known [3] to cause dissolution of cementite, Fe_3C, and $Cr_{23}C_6$, as well as other carbides, some of which may be complex. Variation in the quantities of carbides 1-2 μm in size appears to be related to their precipitation which occurs as temperature decreases in the course of and after forging. The quantity of these carbides increases with the amount of strain. The reason is that nucleation of the carbide phase aims to reduce the energy of grain boundaries [14, 15]. The fine-grained austenitic grain with low circularity is characterized by large bounders with high energy. Carbide precipitation is therefore a favourable process in terms of energy.

Acknowledgements

This paper is one of the results of a project under the EPSILON programme sponsored by the Technology Agency of the Czech Republic in support of applied research and experimental development: TH02020161: Development of high-purity high-alloy steel with ultrafine microstructure and an extreme amount of mechanical working for special applications.

References

[1] Davis J R et al. 1998 Tool materials ASM specialty handbook *ASM international*
[2] Kříž A and Průcha V 2019 Condition of carbides in high-speed steels after multidirectional forging *Defect and Diffusion Forum* Vol. **395** pp. 1-15
[3] Fremunt P, Krejčík J and Podrábský T 1994 Nástrojové oceli (Dům techniky Brno)
[4] European Steel and Alloy Grades/Numbers Searchable Database [online] [Accessed on 25/06/ 2019] *Kharkiv Polytechnic Institute* Aviable from: http://www.steelnumber.com/en/steel_composition_eu.php?name_id=1002Materiálový list.
[5] Material Sheet [online] [Accessed on 25/06/2019] *Bohdan Bolzano* Available from: https://www.bolzano.cz/cz/technicka-podpora/technicka-prirucka/nastrojove-oceli/nastrojove-oceli-rychlorezne/materialove-listy/materialovy-list-oceli-hs-6-5-2-5
[6] Průcha V, Kříž A and Veselý V 2018 Aspects of evaluation of carbide phase in high-speed steels *In Kovárenství (*Brno: Svaz Kováren ČR z.*s*.) No. **65**, pp. 59-63 ISSN: 1213-9289
[7] ISO 16232-7:2007 Road vehicles-Cleanliness of components of fluid circuits: Part 7: Particle sizing and counting by microscopic analysis *Technical Committee ISO/TC 22*
[8] Scientific Forming Technologies Corporation [online] © 2019 Available from: http://deform.com [Accessed on 25/06/2019]
[9] Spittel T and Spittel M. 2009 Ferrous alloys, Volume 2, *Springer*, ISBN 978-3-540-44758-0
[10] Altan T Ngaile G and SHEN G 2005 Cold and hot forging, fundamentals and Applications. *ASM International*
[11] Benešová S and Kesl M 2019 Treatment of high quality forged high-speed steel with ulta-fine structure pro specials tools *Kovárenství,* No. **68**, Svaz kováren České republiky z.s. (Czech Forging Association).
[12] ČSN EN ISO 643 (42 0462) 2014 Ocel - Mikrografické stanovení velikosti zrn. OPRAVA 1. (Praha: Úřad pro technickou normalizaci, metrologii a státní zkušebnictví)
[13] Wojnar L, Kurzydlowski K J and Szala J 2004 *Quantitative Image Analysis*, Metallography and Microstructures*,* Vol 9, *ASM Handbook,(* ASM International), pp. 403–427
[14] Hyspecká L 1983 Teorie tepelného zpracování (VŠB Ostrava)
[15] Smallman R E and Ngan A H W 2007 Physical metalurgy and Advanced Materials *Elsevier Ltd.*